Supplementary Information

Enhancing Electrocatalytic Activity of Metal-Organic Frameworks in Oxygen Evolution Reaction by Introducing High-Valent Metal Centers†

Jie Dong, ‡[a] Danil W. Boukhvalov, ‡[be] Cuncai Lv, [c] Mark G Humphrey, [d] Chi Zhang *[a] and Zhipeng Huang *[a]

[a]China-Australia Joint Research Center for Functional Molecular Materials, School of Chemical Science and Engineering, Tongji University, Shanghai, 200092, China. Email: chizhang@tongji.edu.cn, zphuang@tongji.edu.cn

[b]College of Science, Nanjing Forestry University, Nanjing 210037, China

[c]Key Laboratory of High-precision Computation and Application of Quantum Field Theory of Hebei Province, Hebei Key Lab of Optic-electronic Information and Materials, The College of Physics Science and Technology, Hebei University, Baoding 071002, China

[d]Research School of Chemistry, Australian National University, Canberra, ACT, 2601, Australia

[e]Institute of Physics and Technology, Ural Federal University, Mira Str. 19, 620002 Yekaterinburg, Russia

‡ These authors contributed equally

The specific steps of DFT modeling are as follows:

I: $* + H_2O \rightarrow *OH + H^+ + e^-$

II: $*HO \rightarrow *O + H^+ + e^-$

III: $*O + H_2O \rightarrow *OOH + H^+ + e^-$

IV: $*OOH \rightarrow * + O_2 + H^+ + e^-$

Content

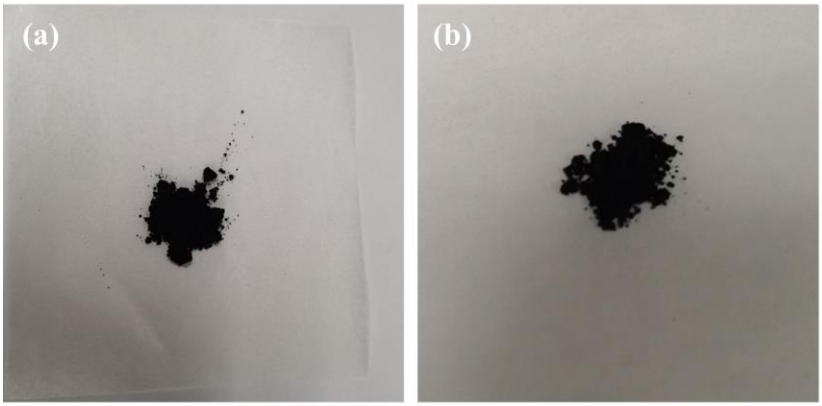

Fig. S1 Optical images of Ni-HHTP-CH and Ni-HHTP-MH.

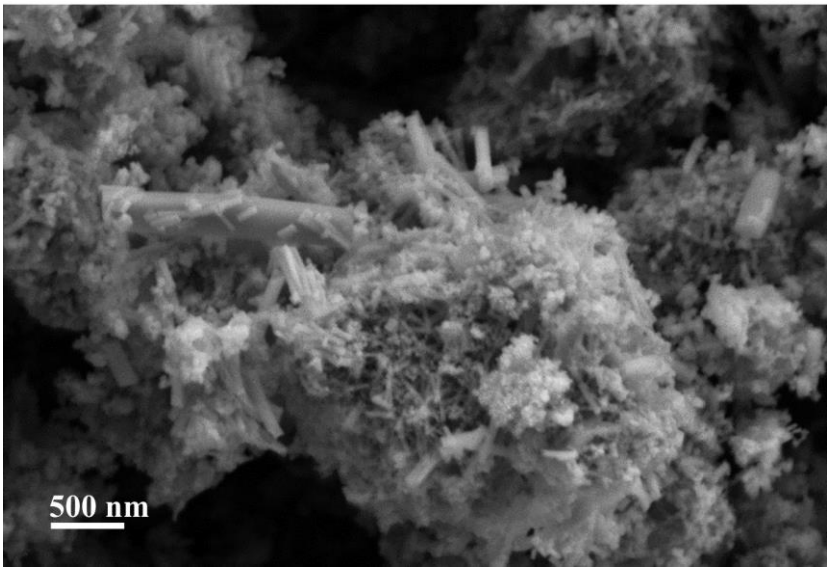

Fig. S2 SEM images of Ni-HHTP-CH.

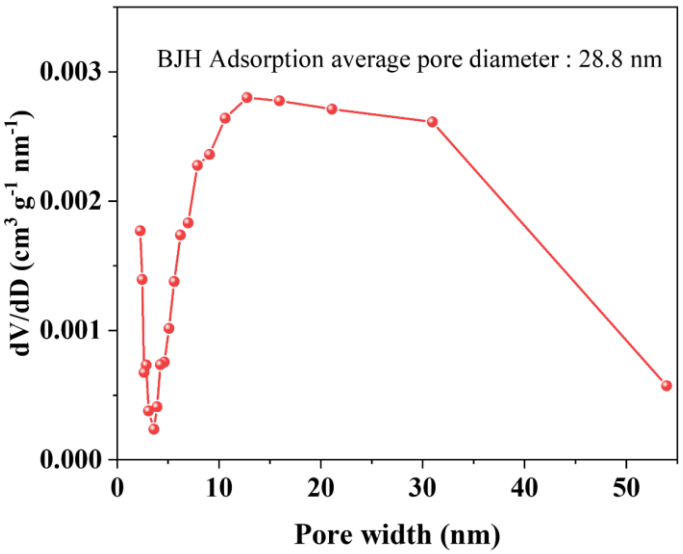

Fig. S3 The pore size distribution curves of the Ni-HHTP-MH.

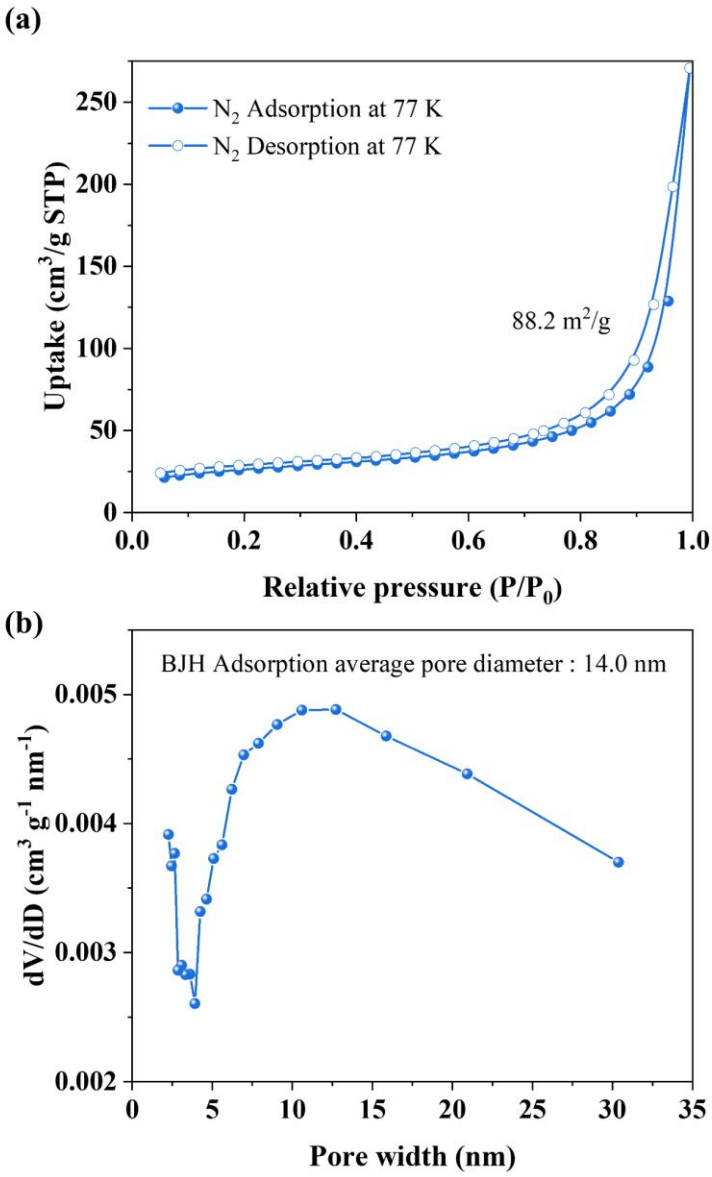

Fig. S4 (a) The N_2 sorption/desorption isotherms and (b) pore size distribution curves of the Ni-HHTP-CH.

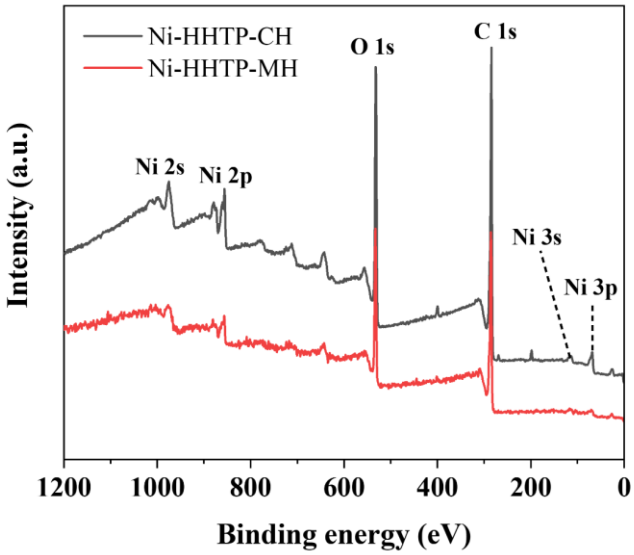

Fig. S5 XPS survey spectra of the Ni-HHTP-CH and Ni-HHTP-MH.

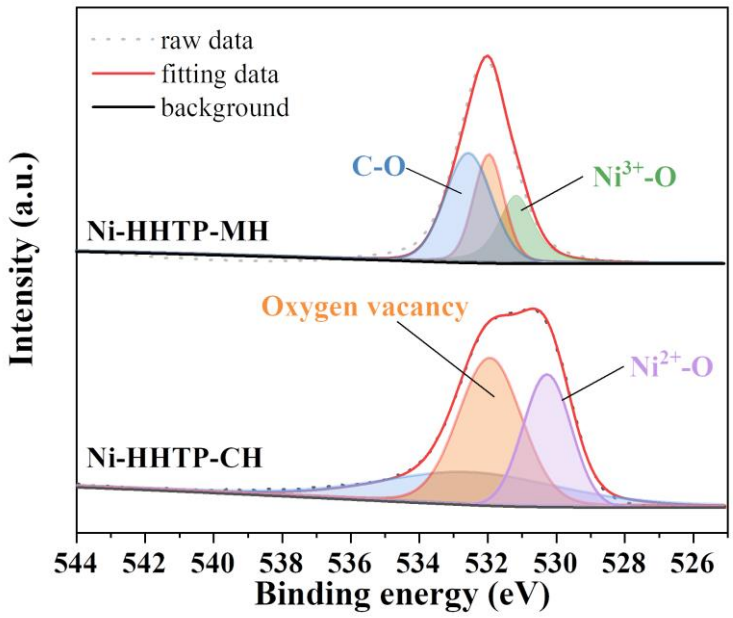

Fig. S6 High-resolution O 1s XPS spectra of the Ni-HHTP-CH and Ni-HHTP-MH.

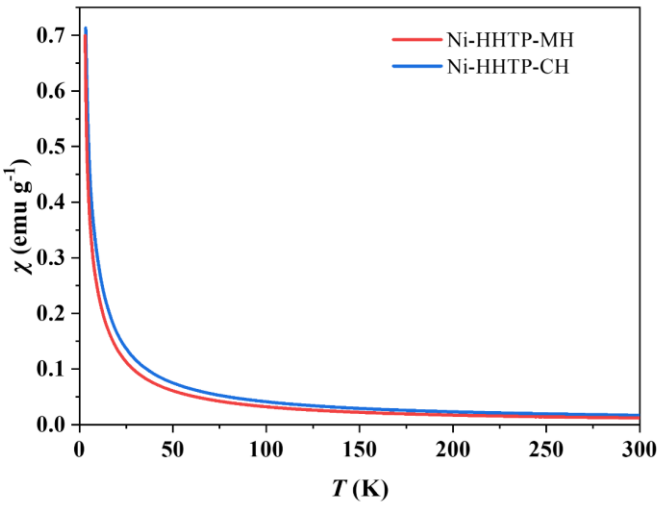

Fig. S7 Magnetic susceptibility of Ni-HHTP-MH and Ni-HHTP-CH.

The total effective magnetic moment (μ_{eff}) can be obtained by fitting the χ^{-1}-T curve according to Langevin theory. The number of unpaired d electrons is further calculated using χ^{-1}-T and is denoted as n. The calculated μ_{eff} values for Ni-HHTP-MH and Ni-HHTP-CH are 2.83 μ_B and 3.57 μ_B, respectively, and Ni ions and radicals contribute both.[1] The magnetic moments (μ) of Ni ions and radicals are abbreviated as μ_{Ni} and μ_{rad}, respectively, by the equation: $\mu_{eff}^2=\mu_{Ni}^2+\mu_{rad}^2$, the μ_{Ni} for Ni-HHTP-MH and Ni-HHTP-CH are derived as 1.77 μ_B and 2.81 μ_B, respectively. Because each building unit of Ni-HHTP contributes 1.33 radicals[2], μ_{rad} for Ni-HHTP can be calculated as 2.10 μ_B. According to the formula: $\mu=\sqrt{n(n+2)}$, the calculated n for Ni-HHTP-MH and Ni-HHTP-CH are 1.03 and 2.00, respectively.

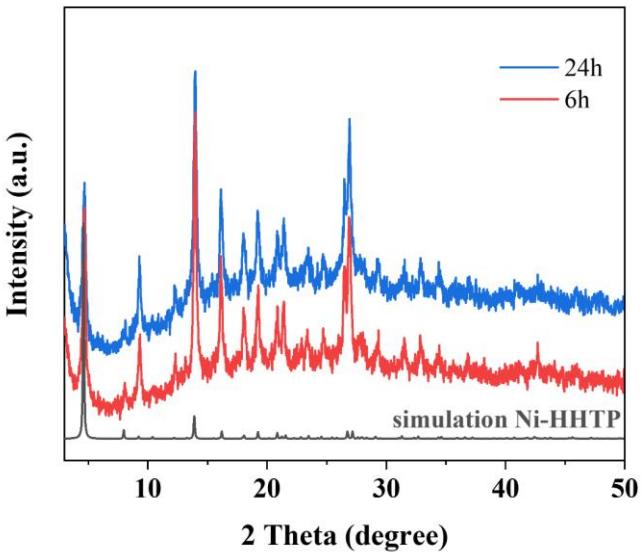

Fig. S8 XRD patterns of Ni-HHTP-CH synthesized at different heating temperatures.

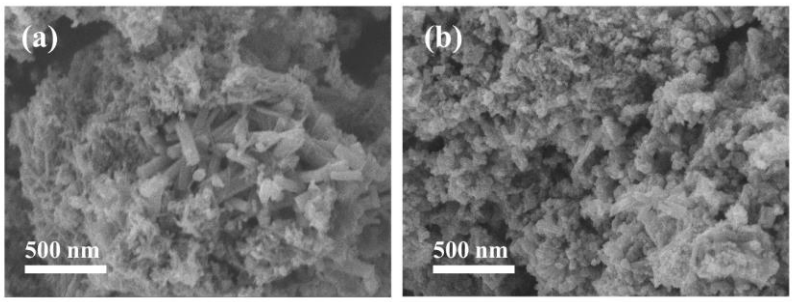

Fig. S9 SEM images of Ni-HHTP-CH synthesized at different heating temperatures: (a) 75 °C and (b) 105 °C.

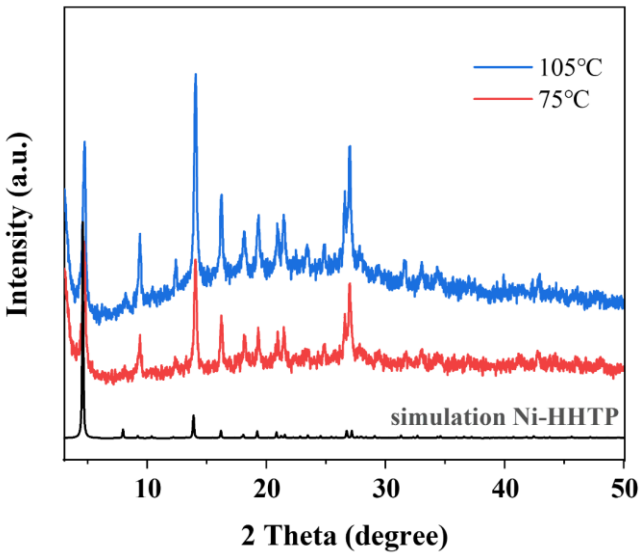

Fig. S10 XRD patterns of Ni-HHTP-CH synthesized at different heating times.

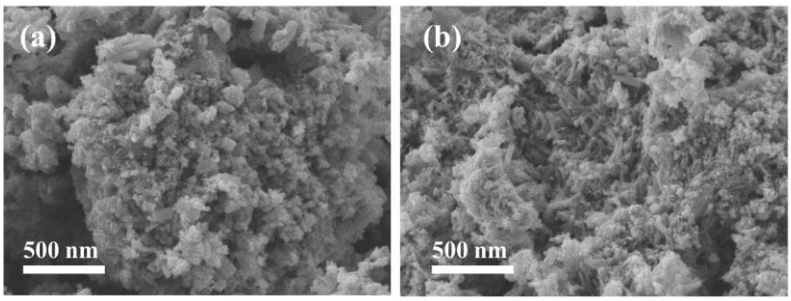

Fig. S11 SEM images of Ni-HHTP-CH synthesized at different heating times: (a) 6 h and (b) 24 h.

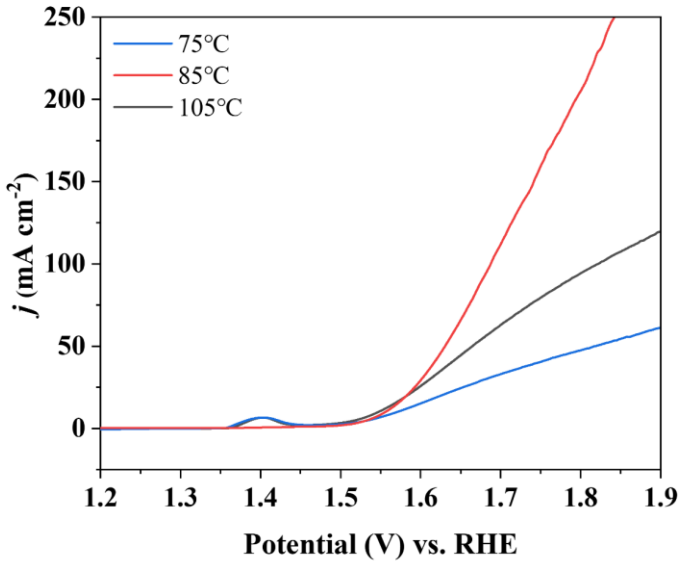

Fig. S12 LSV curves of Ni-HHTP-CH synthesized at different heating temperatures.

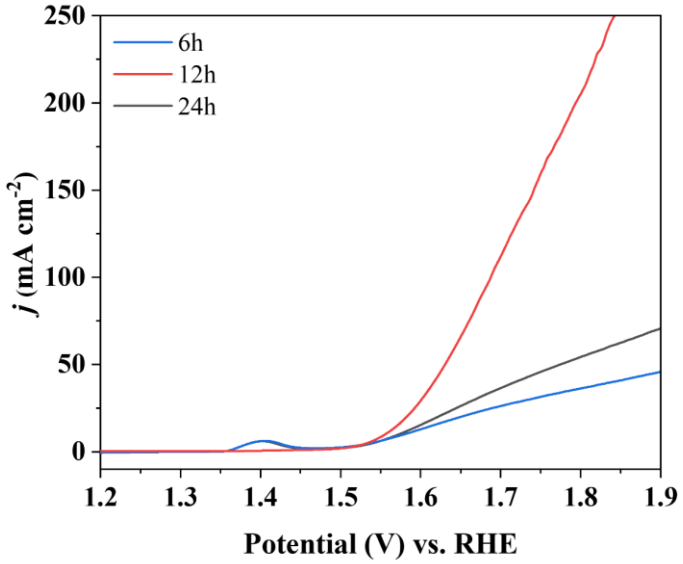

Fig. S13 LSV curves of Ni-HHTP-CH synthesized at different heating times.

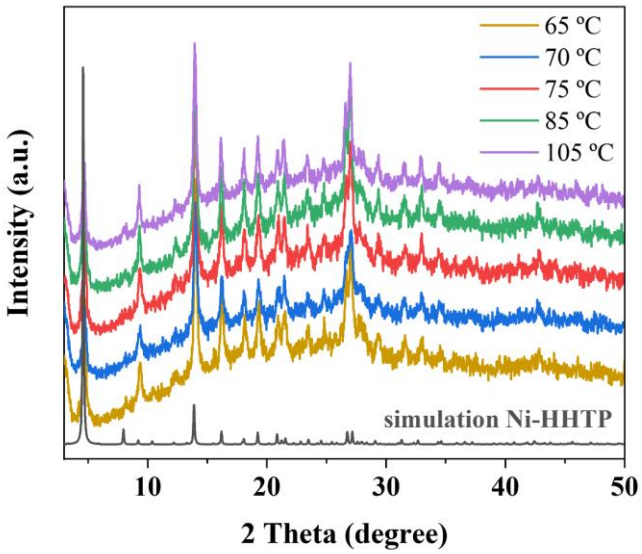

Fig. S14 XRD patterns of Ni-HHTP-MH synthesized at different microwave heating temperatures.

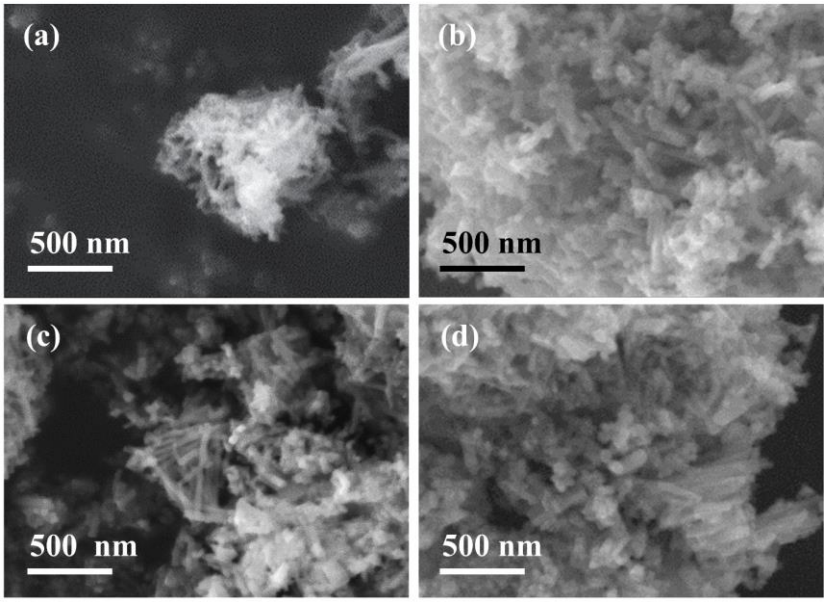

Fig. S15 SEM images of Ni-HHTP-MH synthesized at different microwave heating temperatures: (a) 65 °C, (b) 70 °C, (c) 85 °C and (a) 105 °C.

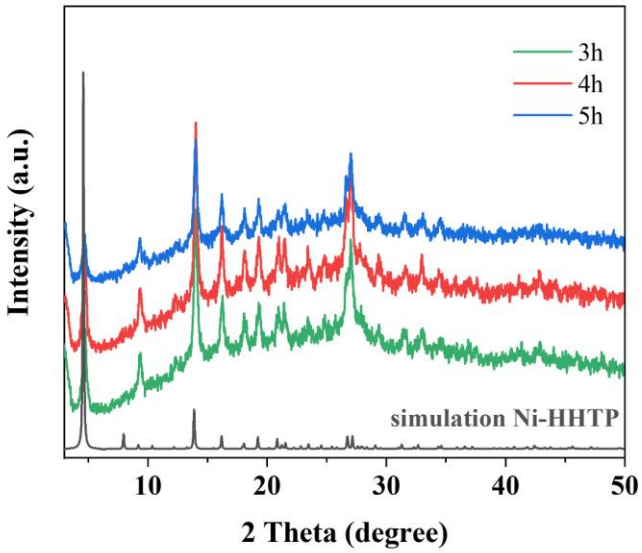

Fig. S16 XRD patterns of Ni-HHTP-MH synthesized at different microwave heating times.

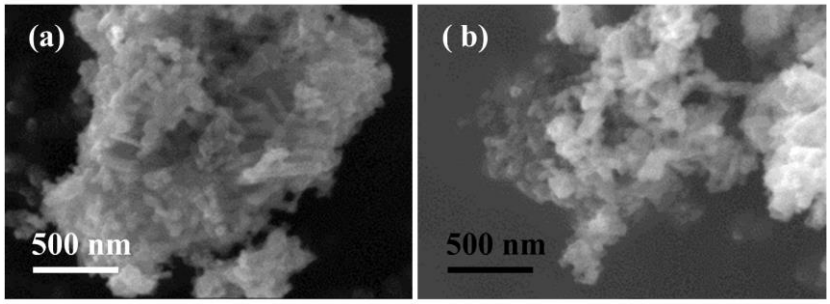

Fig. S17 SEM images of Ni-HHTP-MH synthesized at different microwave heating times: (a) 3 h and (b) 5 h.

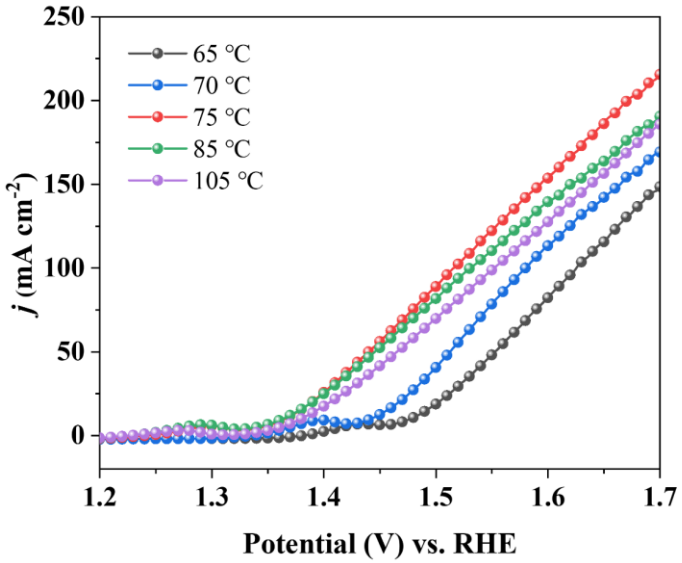

Fig. S18 LSV curves of Ni-HHTP-MH synthesized at different microwave heating temperatures.

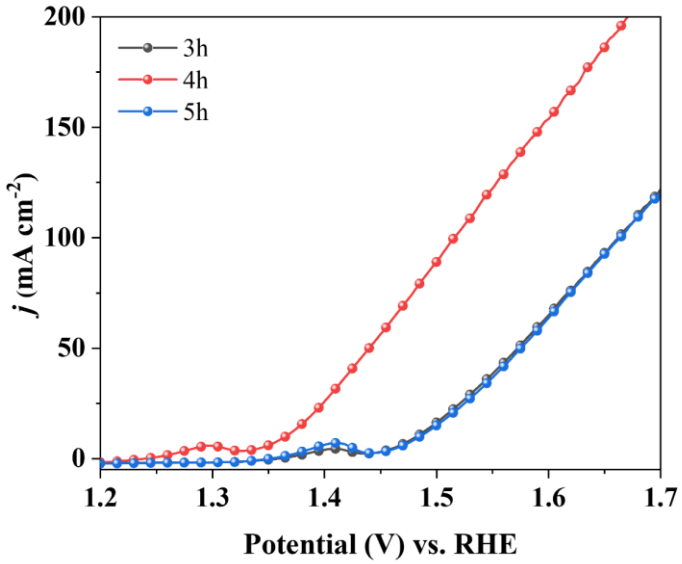

Fig. S19 LSV curves of Ni-HHTP-MH synthesized at different microwave heating times.

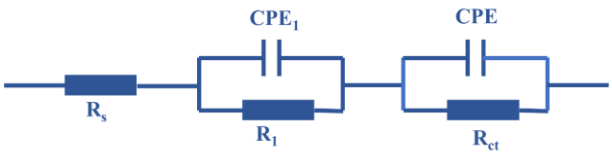

Fig. S20 The equivalent circuit model for electrochemical impedance tests. R_s, R_1, and R_{ct} represent the resistances of the electrolyte, electrode porosity, and charge transfer, respectively. The constant phase angle element (CPE) represents the double-layer capacitance of a solid electrode in a real-world situation.

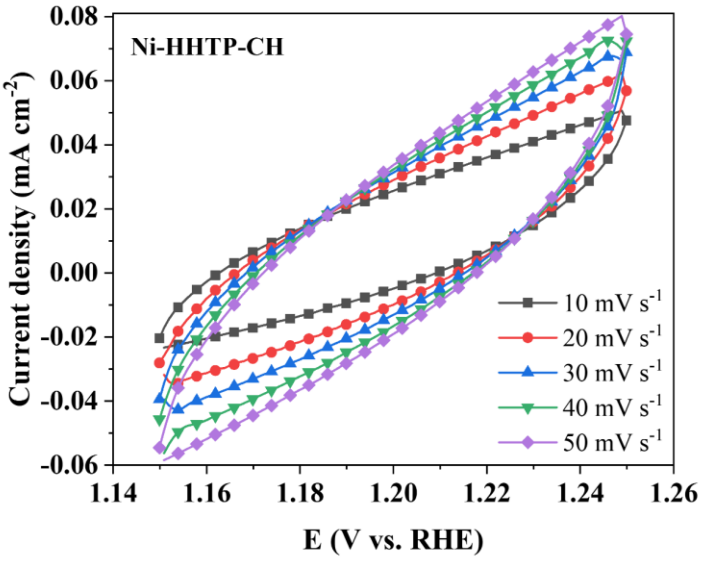

Fig. S21 Cyclic voltammogram of Ni-HHTP-CH in 1.0 M KOH solutions at various scan rates within a potential range of 1.15-1.25 V.

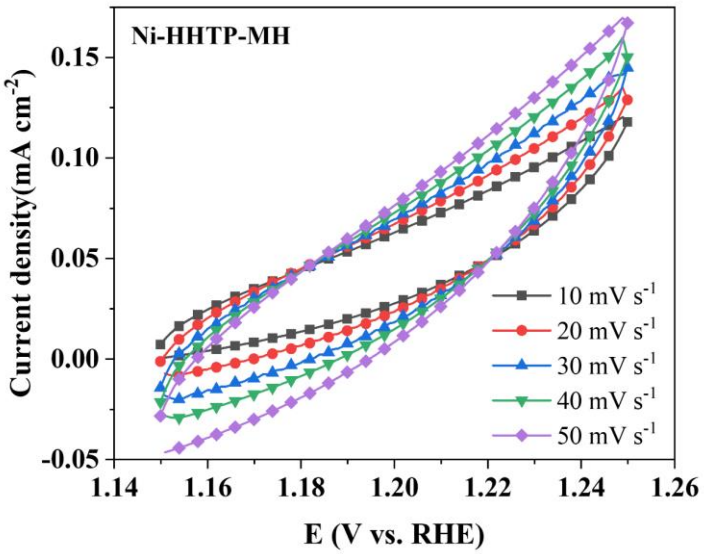

Fig. S22 Cyclic voltammogram of Ni-HHTP-MH in 1.0 M KOH solutions at various scan rates within a potential range of 1.15-1.25 V.

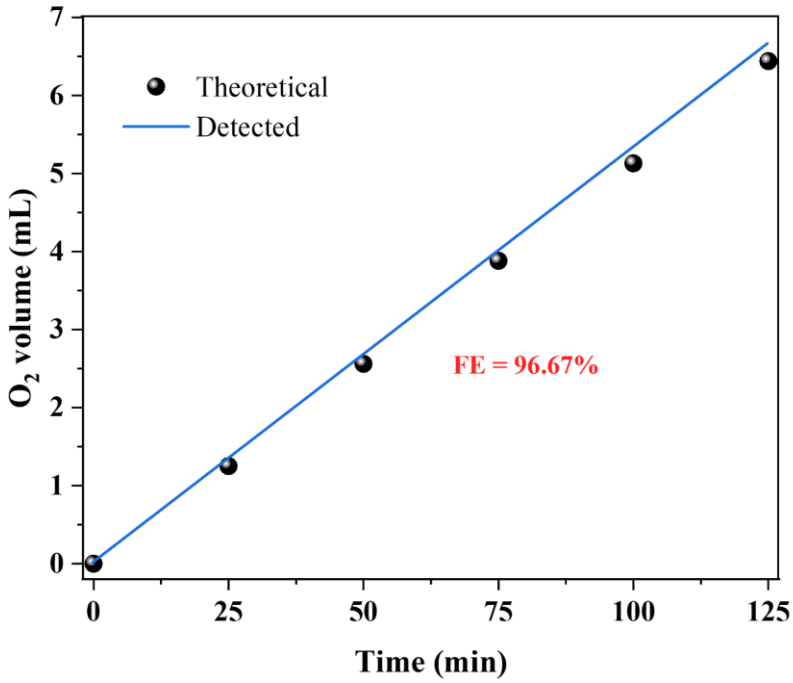

Fig. S23 Diagram of theoretical and detected O_2 volume at a constant current density of 20 mA cm^{-2} in 1.0 M KOH.

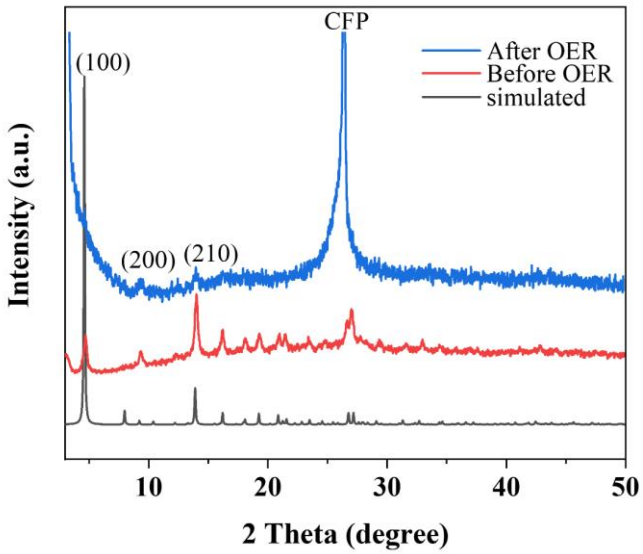

Fig. S24 XRD patterns of Ni-HHTP-MH before and after the OER durability test.

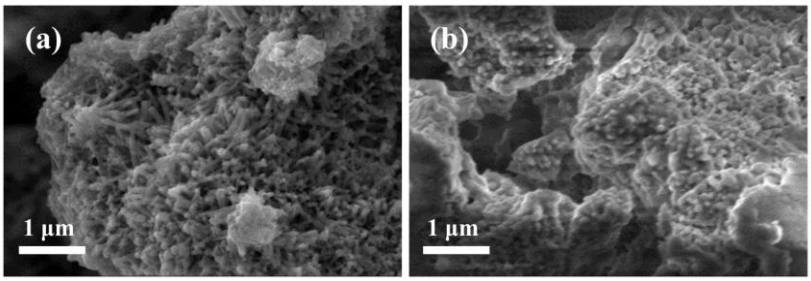

Fig. S25 SEM images of Ni-HHTP-MH before and after the OER durability test.

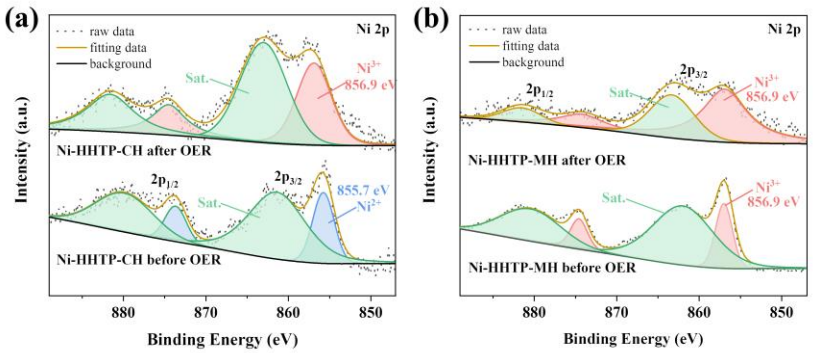

Fig. S26 High-resolution Ni 2p XPS spectra of (a) the Ni-HHTP-CH and (b) the Ni-HHTP-MH before and after the OER test.

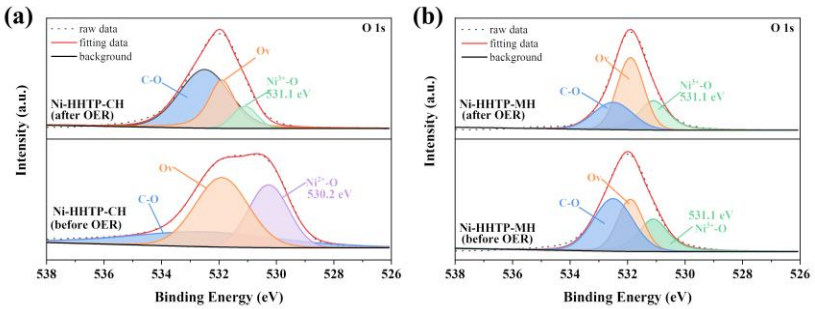

Fig. S27 High-resolution O 1s XPS spectra of (a) the Ni-HHTP-CH and (b) the Ni-HHTP-MH before and after the OER.

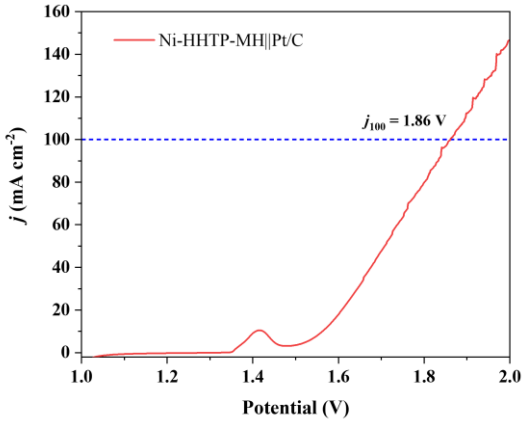

Fig. S28 Overall water splitting performances of Ni-HHTP-MH||Pt/C in 1 M KOH.

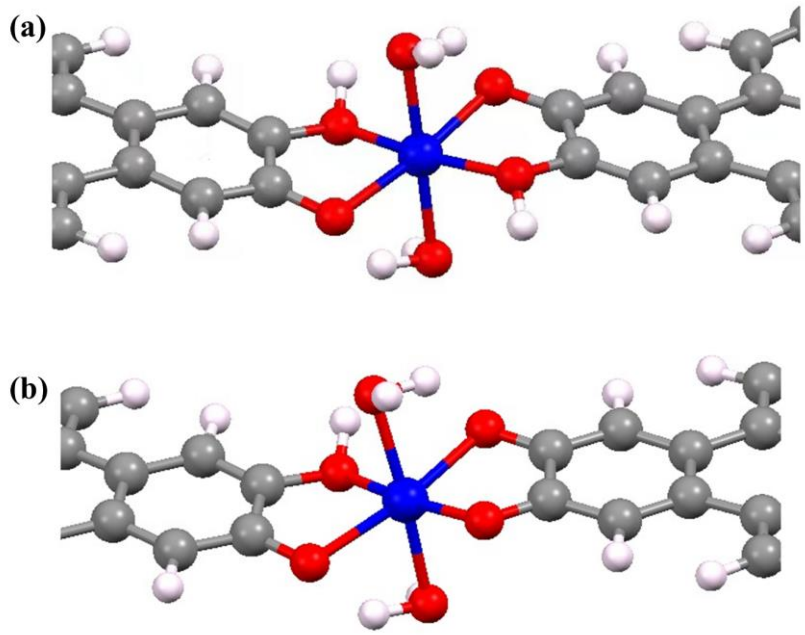

Fig. S29 Optimized geometrical structures of (a) Ni-HHTP-CH and (b) Ni-HHTP-MH. The blue, red, white and grey colors refer to Ni, O, H and C atoms, respectively.

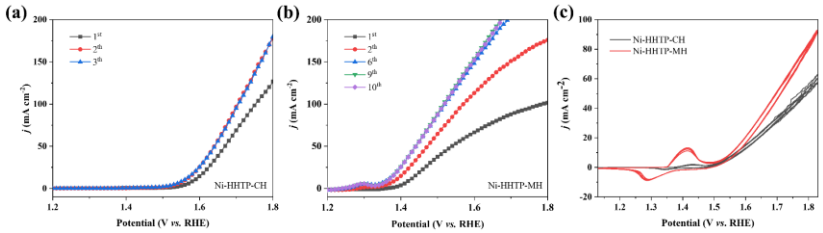

Fig. S30 LSV curves of (a) the Ni-HHTP-CH and (b) the Ni-HHTP-MH; (c) Cyclic voltammetry curves of Ni-HHTP-MH and Ni-HHTP-CH.

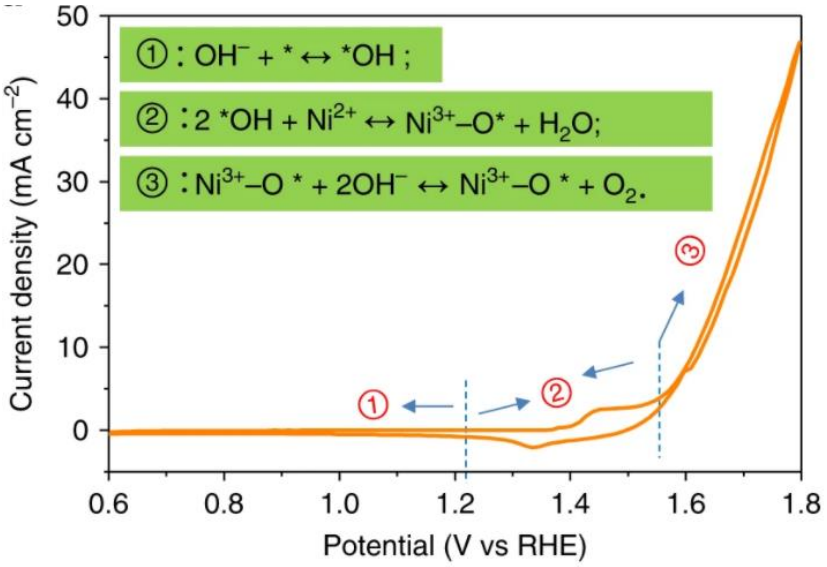

Fig. S31 Cyclic voltammetry for $Ni(OH)_2$ at the potential range of 0.6–1.8 V[3].

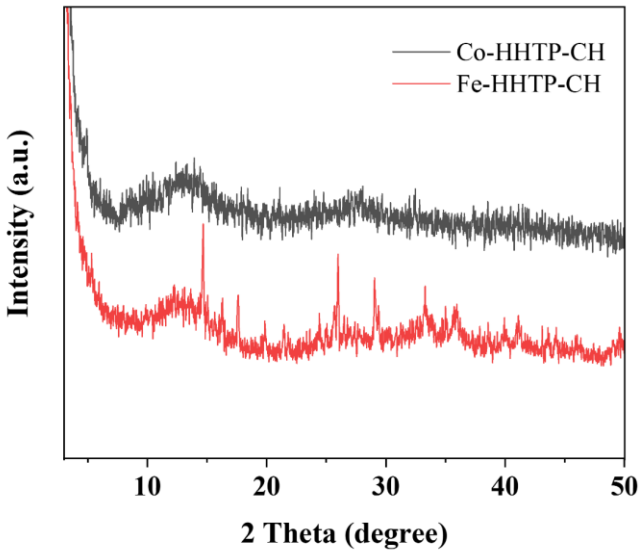

Fig. S32 XRD patterns of Co-HHTP-CH and Fe-HHTP-CH.

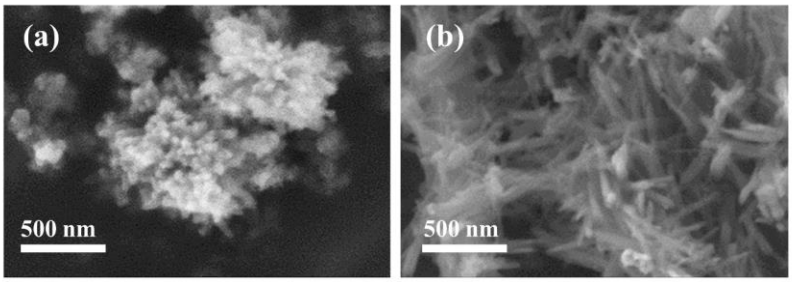

Fig. S33 SEM images of Co-HHTP-MH and Fe-HHTP-MH.

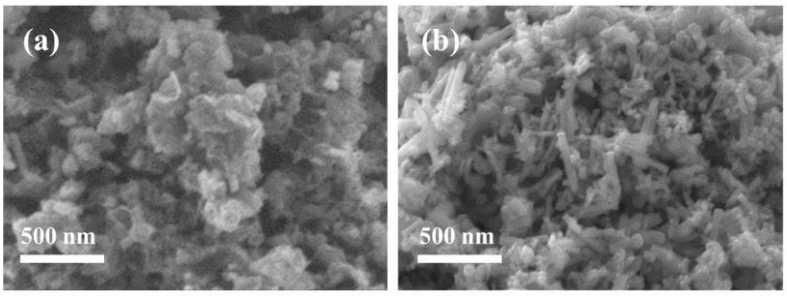

Fig. S34 SEM images of Co-HHTP-CH and Fe-HHTP-CH.

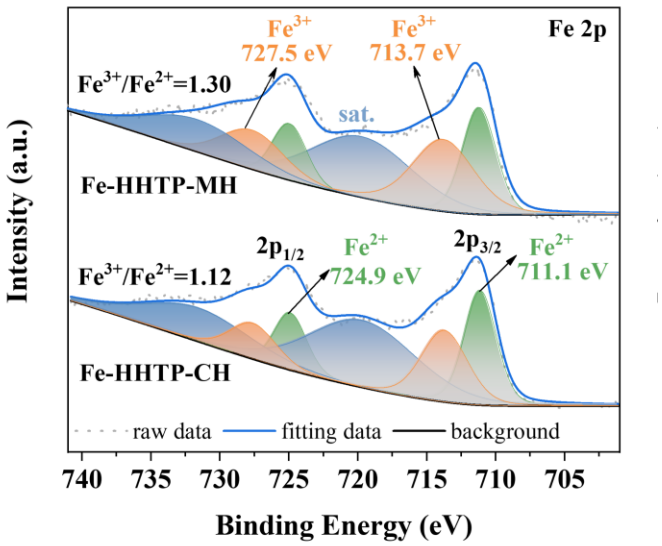

Fig. S35 High-resolution Fe 2p XPS spectra of Fe-HHTP-MH and Fe-HHTP-CH.

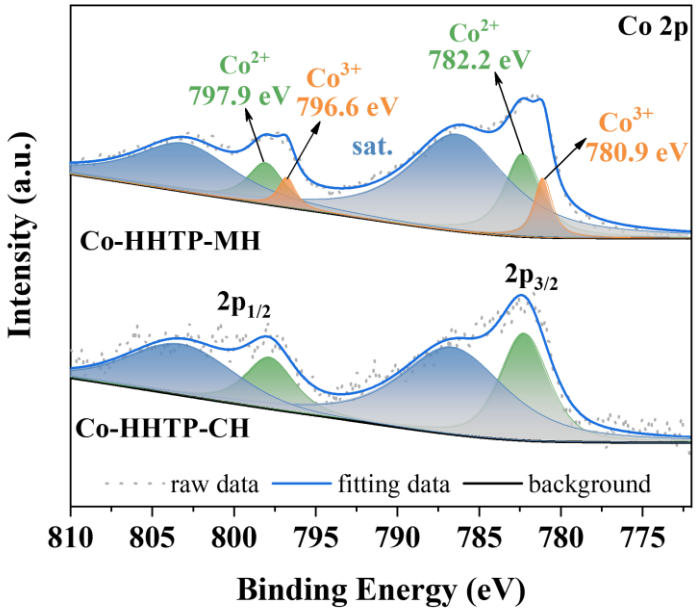

Fig. S36 High-resolution Co 2p XPS spectra of Co-HHTP-MH and Co-HHTP-CH.

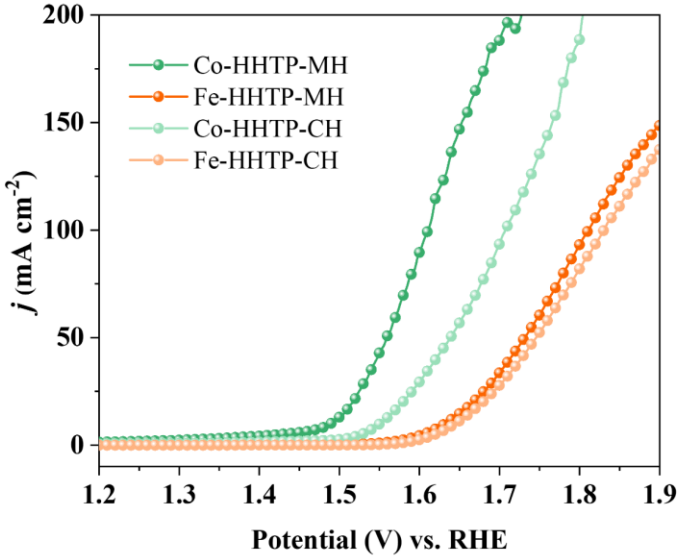

Fig. S37 LSV curves of Co-HHTP-MH, Fe-HHTP-MH, Co-HHTP-CH and Fe-HHTP-CH.

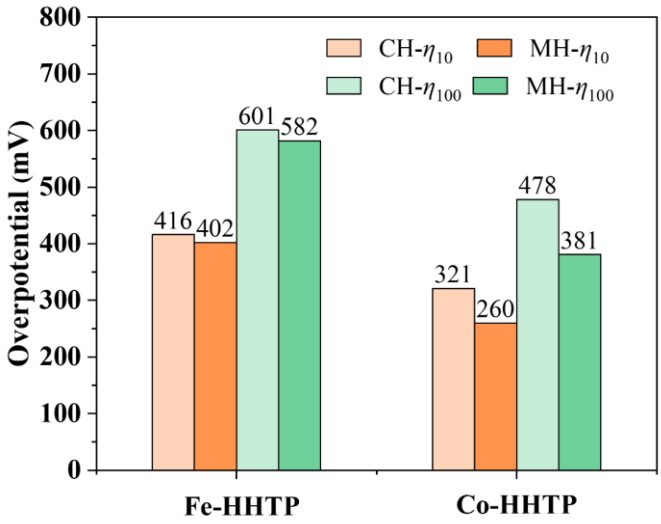

Fig. S38 η_{10} and η_{100} of Co-HHTP-MH, Fe-HHTP-MH, Co-HHTP-CH and Fe-HHTP-CH.

Table S1 The EIS results of Ni-HHTP-MH and Ni-HHTP-CH in 1.0 M KOH solution.

Sample	R_s (Ω)	R_1 (Ω)	R_{ct} (Ω)	CPE (mF)	CPE_1 (mF)
Ni-HHTP-MH	1.313	4.58	17.0	15.75	2.243
Ni-HHTP-CH	1.564	1.67	33.5	8.64	1.781

Table S2 TOF was calculated from the ICP results.

Sample	n (10^{-6} mmol) based on ICP results	TOF calculated from n based on ICP results (s^{-1})
Ni-HHTP-MH	4.56	0.062
Ni-HHTP-CH	4.40	0.002

Table S3 Comparisons of the recently reported OER electrocatalysts based on metal-organic frameworks in alkaline solution.

Catalyst	Scan rate ($mV\ s^{-1}$)	η_{10} (mV)	η_{100} (mV)	Tafel slop ($mV\ dec^{-1}$)	Substrate	Ref.
Ni-HHTP-MH	5	136	286	80.3	CFP	This work
NiFe-NFF	5	227	253	38.9	NFF	4
Pt-NC/Ni-MOF	5	292	-	-	GCE	5
Ni–Fe–MOF	5	221	320	56.0	GCE	6
CoBDC-Fc-NF	2	178	241	51.0	NF	7
MCCF/NiMn-MOFs	5	280	-	86.0	CP	8
CoNi-MOFNA	5	215	250	51.6	CNF	9
FeCo-MOF-EH	2	301	-	42.0	CFP	10
M-PCBN/CC	5	232	270	32.0	CC	11
$Ni_{0.5}Co_{0.5}$-MOF-74	5	198	-	49.0	GCE	12
CoCu-MOF NBs.	5	271	334	63.5	CP	13
2D MOF-Fe/Co(1:2)	10	238	330	52.0	GCE	14
Co-LDH@ZIF-67	5	187	310	59.0	CC	15
NiFc-MOF/NF	10	195	241	48.5	NF	16
NiFe-MOF/G	5	258	328	49.0	GCE	17
NiFe-MOF	5	215	263	49.1	CFC	18
Fe–Co–Ni MOF	5	254	406	51.3	NF	19
Ni-BDC-1R	0.5	225	350	89.0	NF	20
MIL-53(Fe)-2OH	1	215	270	45.4	NF	21
Ni_2Fe_1 Sq-zbr-MOF	5	230	270	37.7	CP	22
NiYCe-MOF/NF	5	245	264	65.0	NF	23

The η_{10} and η_{100} were overpotential at current density of 10 and 100 $mA\ cm^{-2}$; CFP: carbon fiber paper; NFF: NiFe alloy foam; GCE: glassy carbon electrode; NF: nickel foam; CP: carbon paper; CNF: Co_9Ni_1 foam; CC: carbon cloth; CFC: carbon fiber cloth.

Table S4 Comparisons of OER performance of our catalysts to the most active catalysts reported recently in alkaline solution.

Catalyst	Scan rate (mV s^{-1})	η_{10} (mV)	η_{100} (mV)	Tafel slop (mV dec^{-1})	Substrate	Ref.
Ni-HHTP-MH	5	136	286	80.3	CFP	This work
NiFe-P_{Zn}@PNTA	5	172	~290	50.0	PNTA	24
NiOOH/(LDH/α-FeOOH)	5	195	250	35.0	NF	25
TMB@NiNC	1	208	230	41.4	NF	26
$FeCoNiS_x$	1	202	255	47.0	NF	27
CoP/Fe-Co_9S_8	5	156	~250	41.7	NF	28
Ce-NiFe	5	195	~232	22.8	NFF	29
Fe@MoS_2-C	5	194	~325	63.0	NF	30
Ni–Gr–CNTs–Sn_4P_3	5	169@20	375	88.0	NF	31
Au/ULDH−NiFe	5	189	-	35.0	GCE	32
W-$NiS_{0.5}Se_{0.5}$	5	171	239	41.0	NF	33
NiFeV nanofiber	10	181	269	47.0	CC	34
Ru-$NiCo_2S_{4-x}$	2	190@50	~330	61.3	NF	35
Ir/CoNiB	1	178	242	35.1	NF	36
Ir_{SA}-Ni_2P	5	149	~252	90.1	GCE	37

The η_{10} and η_{100} were overpotential at current density of 10 and 100 mA cm^{-2}; CFP: carbon fiber paper; PNTA: porous nickel tube arrays; NF: nickel foam; NFF: NiFe alloy foam; GCE: glassy carbon electrode; CC: carbon cloth.

Reference

1. L. Yang, X. He and M. Dinca, *J. Am. Chem. Soc.*, 2019, **141**, 10475-10480.
2. Q. Lv, Z. Zhu, Y. Ni, J. Geng and F. Li, *Angew. Chem. Int. Ed.*, 2022, **61**, e202114293.
3. J. Q. Yan, L. Q. Kong, Y. J. Ji, J. White, Y. Y. Li, J. Zhang, P. F. An, S. Z. Liu, S. T. Lee and T. Y. Ma, *Nature Commun.*, 2019, **10**, 2149.
4. C. Cao, D.-D. Ma, Q. Xu, X.-T. Wu and Q.-L. Zhu, *Adv. Funct. Mater.*, 2019, **29**, 1807418.
5. C. X. Guo, Y. Jiao, Y. Zheng, J. Luo, K. Davey and S. Z. Qiao, *Chem*, 2019, **5**, 2429-2441.
6. F.-L. Li, P. Wang, X. Huang, D. J. Young, H.-F. Wang, P. Braunstein and J.-P. Lang, *Angew. Chem. Int. Ed.*, 2019, **58**, 7051-7056.
7. Z. Xue, K. Liu, Q. Liu, Y. Li, M. Li, C.-Y. Su, N. Ogiwara, H. Kobayashi, H. Kitagawa, M. Liu and G. Li, *Nat. Commun.*, 2019, **10**, 5048.
8. W. Cheng, X. F. Lu, D. Luan and X. W. Lou, *Angew. Chem. Int. Ed.*, 2020, **59**, 18234-18239.
9. L. Huang, G. Gao, H. Zhang, J. X. Chen, Y. X. Fang and S. J. Dong, *Nano Energy*, 2020, **68**, 104296.
10. J. Tian, F. Jiang, D. Yuan, L. Zhang, Q. Chen and M. Hong, *Angew. Chem. Int. Ed.*, 2020, **59**, 13101-13108.
11. W. Zhang, Y. Wang, H. Zheng, R. Li, Y. Tang, B. Li, C. Zhu, L. You, M.-R. Gao, Z. Liu, S.-H. Yu and K. Zhou, *ACS Nano*, 2020, **14**, 1971-1981.
12. S. Zhao, C. Tan, C.-T. He, P. An, F. Xie, S. Jiang, Y. Zhu, K.-H. Wu, B. Zhang, H. Li, J. Zhang, Y. Chen, S. Liu, J. Dong and Z. Tang, *Nat. Energy*, 2020, **5**, 881-890.
13. W. Cheng, Z.-P. Wu, D. Luan, S.-Q. Zang and X. W. Lou, *Angew. Chem. Int. Ed.*, 2021, **60**, 26397-26402.
14. K. Ge, S. Sun, Y. Zhao, K. Yang, S. Wang, Z. Zhang, J. Cao, Y. Yang, Y. Zhang, M. Pan and L. Zhu, *Angew. Chem. Int. Ed.*, 2021, **60**, 12097-12102.
15. Z. Li, X. Zhang, Y. Kang, C. C. Yu, Y. Wen, M. Hu, D. Meng, W. Song and Y. Yang, *Adv. Sci.*, 2021, **8**.
16. J. Liang, X. Gao, B. Guo, Y. Ding, J. Yan, Z. Guo, E. C. M. Tse and J. Liu, *Angew. Chem. Int. Ed.*, 2021, **60**, 12770-12774.
17. Y. Wang, B. Liu, X. Shen, H. Arandiyan, T. Zhao, Y. Li, M. Garbrecht, Z. Su, L. Han, A. Tricoli and C. Zhao, *Adv. Energy Mater.*, 2021, **11**, 2003759.
18. J. Zhou, Z. Han, X. Wang, H. Gai, Z. Chen, T. Guo, X. Hou, L. Xu, X. Hu, M. Huang, S. V. Levchenko and H. Jiang, *Adv. Funct. Mater.*, 2021, **31**, 2102066.
19. F. S. Farahani, M. S. Rahmanifar, A. Noori, M. F. El-Kady, N. Hassani, M. Neek-Amal, R. B. Kaner and M. F. Mousavi, *J. Am. Chem. Soc.*, 2022, **144**, 3411-3428.
20. L. Zhang, J. Wang, K. Jiang, Z. Xiao, Y. Gao, S. Lin and B. Chen, *Angew. Chem. Int. Ed.*, 2022, **61**, e202214794.
21. C. Zhang, Q. Qi, Y. Mei, J. Hu, M. Sun, Y. Zhang, B. Huang, L. Zhang and S. Yang, *Adv. Mater.*, 2022, e2208904.
22. S. Kandambeth, V. S. Kale, D. Fan, J. A. Bau, P. M. Bhatt, S. Zhou, A. Shkurenko, M. Rueping, G. Maurin, O. Shekhah and M. Eddaoudi, *Adv. Energy Mater.*, 2022, **13**, 2202964.
23. F. Li, M. Jiang, C. Lai, H. Xu, K. Zhang and Z. Jin, *Nano Lett.*, 2022, **22**, 7238-7245.
24. Y. Zhou, N. Jin, Y. Ma, Y. Cui, L. Wang, Y. Kwon, W. K. Lee, W. Zhang, H. Ge and J. Zhang, *Adv. Mater.*, 2022, e2209500.
25. M. Cai, Q. Zhu, X. Wang, Z. Shao, L. Yao, H. Zeng, X. Wu, J. Chen, K. Huang and S. Feng, *Adv. Mater.*, 2022, e2209338.
26. M. Moloudi, A. Noori, M. S. Rahmanifar, Y. Shabangoli, M. F. El-Kady, N. B. Mohamed, R. B. Kaner and M. F. Mousavi, *Adv. Energy Mater.*, 2022, **13**, 2203002.
27. A. Wang, X. Zhang, S. Gao, C. Zhao, S. Kuang, S. Lu, J. Niu, G. Wang, W. Li, D. Chen, H. Zhang, X. Zhou, S. Zhang, B. Zhang and W. Wang, *Adv. Mater.*, 2022, **34**, e2204247.
28. X. Chen, Y. Cheng, Y. Wen, Y. Wang, X. Yan, J. Wei, S. He and J. Zhou, *Adv. Sci.*, 2022, **9**, e2204742.
29. J. Liu, Y. Liu, X. Mu, H. Jang, Z. Lei, S. Jiao, P. Yan, M. G. Kim and R. Cao, *Adv. Funct. Mater.*, 2022, **32**, 2204086.
30. F. Gong, M. Liu, L. Gong, S. Ye, Q. Jiang, G. Zeng, X. Zhang, Z. Peng, Y. Zhang, S. Fang and J. Liu, *Adv. Funct. Mater.*, 2022, **32**, 2202141.

31. S. Riyajuddin, M. Pahuja, P. K. Sachdeva, K. Azmi, S. Kumar, M. Afshan, F. Ali, J. Sultana, T. Maruyama, C. Bera and K. Ghosh, *ACS Nano*, 2022, **16**, 4861-4875.
32. S. Kitano, T. G. Noguchi, M. Nishihara, K. Kamitani, T. Sugiyama, S. Yoshioka, T. Miwa, K. Yoshizawa, A. Staykov and M. Yamauchi, *Adv. Mater.*, 2022, **34**, e2110552.
33. Y. Wang, X. Li, M. Zhang, J. Zhang, Z. Chen, X. Zheng, Z. Tian, N. Zhao, X. Han, K. Zaghib, Y. Wang, Y. Deng and W. Hu, *Adv. Mater.*, 2022, **34**, e2107053.
34. B. Zhang, Z. Wu, W. Shao, Y. Gao, W. Wang, T. Ma, L. Ma, S. Li, C. Cheng and C. Zhao, *Angew. Chem. Int. Ed.*, 2022, **61**, e202115331.
35. H. Su, S. Song, Y. Gao, N. Li, Y. Fu, L. Ge, W. Song, J. Liu and T. Ma, *Adv. Funct. Mater.*, 2021, **32**, 2109731.
36. C. Wang, P. Zhai, M. Xia, Y. Wu, B. Zhang, Z. Li, L. Ran, J. Gao, X. Zhang, Z. Fan, L. Sun and J. Hou, *Angew. Chem. Int. Ed.*, 2021, **60**, 27126-27134.
37. Q. Wang, Z. Zhang, C. Cai, M. Wang, Z. L. Zhao, M. Li, X. Huang, S. Han, H. Zhou, Z. Feng, L. Li, J. Li, H. Xu, J. S. Francisco and M. Gu, *J. Am. Chem. Soc.*, 2021, **143**, 13605-13615.